THE JOURNAL OF BIOLOGICAL CHEMISTRY VOL. 288, NO. 42, pp. 30064–30074, October 18, 2013
Published in the U.S.A.

Steap4 Plays a Critical Role in Osteoclastogenesis *in Vitro* by Regulating Cellular Iron/Reactive Oxygen Species (ROS) Levels and cAMP Response Element-binding Protein (CREB) Activation*

Received for publication, April 18, 2013, and in revised form, August 15, 13 Published, JBC Papers in Press, August 29, 2013, DOI 10.1074/jbc.M113.478750

Jian Zhou[1], **Shiqiao Ye**[1], **Toshifumi Fujiwara, Stavros C. Manolagas, and Haibo Zhao**[2]

From the Center for Osteoporosis and Metabolic Bone Diseases, Division of Endocrinology and Metabolism, Department of Internal Medicine, University of Arkansas for Medical Sciences and the Central Arkansas Veterans Healthcare System, Little Rock, Arkansas 72205

Background: Iron uptake through the transferrin-dependent pathway is essential for osteoclast differentiation.
Results: Knocking down the expression of Steap4, an endosomal ferrireductase, inhibits osteoclast formation and decreases cellular iron and ROS production.
Conclusion: Steap4 regulates cellular iron metabolism during osteoclast differentiation.
Significance: This work provides new insights into the molecular mechanisms regulating cellular iron metabolism in osteoclast lineage cells.

Iron is essential for osteoclast differentiation, and iron overload in a variety of hematologic diseases is associated with excessive bone resorption. Iron uptake by osteoclast precursors via the transferrin cycle increases mitochondrial biogenesis, reactive oxygen species production, and activation of cAMP response element-binding protein, a critical transcription factor downstream of receptor activator of NF-κB-ligand-induced calcium signaling. These changes are required for the differentiation of osteoclast precursors to mature bone-resorbing osteoclasts. However, the molecular mechanisms regulating cellular iron metabolism in osteoclasts remain largely unknown. In this report, we provide evidence that Steap4, a member of the six-transmembrane epithelial antigen of prostate (Steap) family proteins, is an endosomal ferrireductase with a critical role in cellular iron utilization in osteoclasts. Specifically, we show that Steap4 is the only Steap family protein that is up-regulated during osteoclast differentiation. Knocking down Steap4 expression *in vitro* by lentivirus-mediated short hairpin RNAs inhibits osteoclast formation and decreases cellular ferrous iron, reactive oxygen species, and the activation of cAMP response element-binding protein. These results demonstrate that Steap4 is a critical enzyme for cellular iron uptake and utilization in osteoclasts and, thus, indispensable for osteoclast development and function.

Osteoclasts are highly specialized, multinucleated cells capable of resorbing calcified cartilage and bone matrix during skeletal development, growth, and remodeling (1, 2). Osteoclastic bone resorption is essential for bone and mineral homeostasis under physiological conditions. Exaggerated bone resorption, either because of increased osteoclast number or enhanced activity, leads to pathological bone loss and is the culprit of metabolic bone diseases such as postmenopausal osteoporosis, Paget disease of bone, rheumatoid arthritis, periodontal disease, and tumor bone metastasis (3).

Osteoclasts originate from mononuclear progenitors of the macrophage lineage that eventually fuse to form polykaryons in a multistep process that is controlled by two indispensible cytokines: the macrophage colony-stimulating factor (M-CSF)[3] and the receptor activator of NF-κB ligand (RANKL) (4). M-CSF stimulates the proliferation of macrophages and the survival of the mature osteoclast polykaryons by activating ERK and the PI3K/AKT pathways (5). RANKL, on the other hand, induces the expression of osteoclast-specific genes and promotes the survival of mature osteoclasts by activating NF-κB, MAPKs, and PI3K/AKT (1). In addition, RANKL stimulates $[Ca^{2+}]_i$ oscillation in osteoclast precursors, and $[Ca^{2+}]_i$, in turn, activates calcineurin and a calmodulin-dependent kinase-CREB pathway, resulting in the induction and activation of nuclear factor of activated T-cells, cytoplasmic, calcineurin-dependent 1 (NFATc1), the master transcription factor for osteoclastogenesis (6, 7). Activation of CREB during osteoclast differentiation induces the expression of the peroxisome proliferator-activated receptor γ coactivator 1β (PGC-1β). PGC-1β then acts to stimulate mitochondrion biogenesis and the generation of reactive oxygen species (ROS), which promote osteoclastogenesis by increasing the activity of CREB and PGC-1β in a positive feedback manner (8, 9).

* This work was supported, in whole or in part, by NIAMS and NIA, National Institutes of Health Grants AR055694, AR062012, and P01 AG13918. This work was also partially supported by University of Arkansas for Medical Sciences Tobacco Settlement Funds provided by the Arkansas Biosciences Institute.

[1] Both authors contributed equally to this work.

[2] To whom correspondence should be addressed: Center for Osteoporosis and Bone Metabolic Diseases, Div. of Endocrinology and Metabolism, Dept. of Internal Medicine, University of Arkansas for Medical Sciences, 4301 W. Markham St., Slot 587, Little Rock, AR 72205. Tel.: 501-686-5130; Fax: 501-686-8148; E-mail: hzhao@uams.edu.

[3] The abbreviations used are: M-CSF, the macrophage colony-stimulating factor; RANKL, receptor activator of NF-κB ligand; CREB, cAMP response element-binding protein; ROS, reactive oxygen species; Tf, transferrin; TfR1, transferrin receptor 1; α-MEM, α-minimal essential medium; BMM, bone marrow macrophage; TRAP, tartrate-resistant acid phosphatase; PG SK, Phen Green SK; pOC, preosteoclast; OC, mature osteoclast; 2,2′-DPD, 2,2′-dipyridyl.

Iron uptake through the transferrin/transferrin receptor (Tf/TfR1) pathway also augments osteoclastogenesis, and the effects of iron are mediated, at least in part, by ROS (8). However, the molecular details of iron homeostasis in osteoclasts are largely unknown, as are the molecular mechanism(s) by which iron overload leads to pathologic bone resorption.

In the extracellular fluid, ferric iron (Fe^{3+}) is mainly bound to Tf with high affinity. Most mammalian cells acquire iron through the Tf cycle, in which iron-loaded Tf binds to TfR on the cell surface, and the complex is then internalized via receptor-mediated endocytosis (10, 11). Fe^{3+} is released from Tf because of acidic pH in endosomes. The Tf-TfR1 complex returns to the plasma membrane and is ready for another round of iron uptake. Before Fe^{3+} can be transported across the endosomal membrane to the cytoplasm, it must be reduced to ferrous iron (Fe^{2+}). The six-transmembrane epithelial antigen of prostate (Steap) family of proteins has been recently identified as ferrireductases responsible for the reduction of Fe^{3+} in mammalian cells (12). Three of the four Steap family members, Steap2, Steap3, and Steap4, are ferric and cupric reductases (13). Notably, mutations in Steap3 in humans and mice lead to microcytic hypochromic anemia, which is caused by deficient iron uptake in erythroid cells (14). Steap1 and Steap2 are highly expressed in the prostate and have been implicated in prostate cancer metastasis (15, 16). Steap4, also known as Stamp2 or Tiarp/Tnfaip9, is highly induced by TNF-α in adipocytes (17, 18), where it regulates insulin sensitivity, glucose metabolism, and inflammation (19). Heretofore, it remains unknown whether Steap family proteins are expressed in osteoclasts and whether they play a role in iron uptake in this cell type.

Mitochondria are the primary consumers of cellular iron for the synthesis of heme and iron-sulfur clusters. Iron is also an integral element in protein complexes along the mitochondrial respiratory chain, which generates adenosine triphosphate for cellular energy metabolism and produces ROS (20). At high concentrations, ROS damage DNA, lipids, and proteins and, thus, cause oxidative stress, one of the major factors implicated in aging and age-associated diseases such as atherosclerosis, arthritis, and type 2 diabetes mellitus (21). On the other hand, at lower nontoxic levels, ROS serve as signaling modifiers in various receptor pathways (22, 23). In macrophages and mature osteoclasts, RANKL signaling increases the intracellular level of ROS, which, in turn, modulate RANKL-induced activation of NF-κB, MAPKs, PI3K/AKT, and calcium oscillations (24–26). ROS are required for optimal osteoclastogenesis and bone resorption and evidently mediate the bone loss caused by sex steroid deficiency (27, 28).

In the work reported here, we have elucidated that Steap4 is an important endosomal ferrireductase in osteoclast lineage cells, responsible for the conversion of ferric iron into ferrous iron for cellular usage. Knocking down Steap4 expression in macrophages inhibits osteoclast formation and decreases cellular ferrous iron concentration, which, in turn, reduces mitochondria ROS production and RANKL-induced CREB activation. Therefore, increased Steap4 expression, working in concert with the up-regulated Tf/TfR pathway identified previously, promotes cellular iron uptake and utilization to cope with the increased iron demand during osteoclast development and function.

EXPERIMENTAL PROCEDURES

Antibodies and Reagents—Commercially available antibodies were as follows: mouse monoclonal anti-actin (GenScript); mouse monoclonal anti-cathepsin K (clone 182-12G5, Millipore); rabbit polyclonal anti-phospho-CREB (catalog no. 9191) and rabbit monoclonal anti-total-CREB (catalog no. 4820) (Cell Signaling Technology); rabbit polyclonal anti-EEA1 (Sigma-Aldrich); mouse monoclonal anti-HA (Covance); mouse monoclonal anti-NFATc1 (catalog no. sc-7294, Santa Cruz Biotechnology); rabbit polyclonal anti-PGC-1β antibody (catalog no. ab130741, Abcam); mouse monoclonal anti-human transferrin receptor (Invitrogen); mouse monoclonal anti-α-tubulin (clone DM1A, Sigma-Aldrich); rabbit polyclonal anti-ERK1/2 and mouse monoclonal anti-phospho-ERK1/2 (Thr-202/Tyr-204), mouse monoclonal anti-AKT (pan) (clone 40D4) and rabbit monoclonal anti-phospho-AKT (Ser-473) (clone 193H12), rabbit polyclonal anti-JNK and mouse monoclonal anti-phospho-JNK (Thr-183/Tyr-185) (clone G9), and rabbit polyclonal anti-IKB-α and mouse monoclonal anti-phospho-IKB-α (Ser-32/36) (clone 5A5) (Cell Signaling Technology).

Cell Culture α-minimal essential medium (α-MEM) and 10 × penicillin-streptomycin-L-glutamine were purchased from Invitrogen and Sigma-Aldrich, respectively. Fetal bovine serum was purchased from Hyclone. Phen Green™ SK, diacetate (catalog no. P14313), and CM-H2DCFDA (catalog no. C6827) were purchased from Molecular Probes. 2,2′-DPD (catalog no. D216305) was purchased from Sigma-Aldrich. MitoSOX Red was bought from Invitrogen.

Bone Marrow Macrophage and Osteoclast Cultures—Bone marrow macrophages (BMMs) were prepared as described previously (29). Briefly, whole bone marrow was isolated from tibiae and femora of 8- to 10-week-old C57/BL6 mice. Bone marrow cells were plated in α-10 medium (α-MEM, 10% heat-inactivated fetal bovine serum, 1 × penicillin-streptomycin-L-glutamine solution) containing 1/10 volume of CMG 14-12 (conditioned medium supernatant containing recombinant M-CSF at 1 μg/ml) (30) in Petri dishes. Cells were incubated at 37 °C in 5% CO_2, 95% air for 4–5 days. Fresh media and CMG 14-12 supernatant were replaced every the other day. Osteoclasts were generated after 5 days of culture of BMMs with 1/100 volume of CMG 14-12 supernatant and 100 ng/ml of recombinant RANKL.

Quantitative Real-time RT-PCR—BMMs were cultured in 6-well plates with M-CSF and/or RANKL for 5 days. Total RNA was purified using an RNeasy mini kit (Qiagen) according to the protocol of the manufacturer. First-strand cDNAs were synthesized from 0.5–1 μg of total RNA using the high-capacity cDNA reverse transcription kit (Invitrogen) following the instructions of the manufacturer. TaqMan quantitative real-time PCR was performed using the following primers from Invitrogen: *Steap1* (Mm00459097_m1), *Steap2* (Mm00459312_m1), *Steap3* (Mm01287243_m1), *Steap4* (Mm00475405_m1), *Acadm* (Mm01323360_g1), *Acp5* (Mm00475698_m1), *ATP5b* (Mm00443967_g1), *Calcr* (Mm00432282_m1), *COX-I* (Mm04225243_g1), *COX-III* (Mm0422526_g1), *COX-VIIa1* (Mm00438297_g1), *Ctsk* (Mm00484039_m1), *NFATc1* (Mm00479445_m1), *PGC-1β* (Mm00504720_m1), *TNFα* (Mm00443260_g1), and *Mrps2* (Mm03991065_g1). Samples were amplified using the StepOne-

Plus real-time PCR system (Invitrogen) with an initial denaturation at 95 °C for 10 min, followed by 40 cycles of 95 °C for 15 s and 60 °C for 1 min. The relative mRNA amounts were calculated by normalizing to the mitochondrial gene Mrps2 mRNA, which is steadily expressed in both BMMs and osteoclasts, using the ΔCt method (31).

Lentivirus-mediated shRNA Expression—The LKO.1 lentiviral vector expressing the shRNA sequence targeting mRNA of murine *Steap4* (TRCN0000249065/NM_054098.3–370s21c1) (Steap4-sh1) was purchased from Sigma-Aldrich. A second Steap4-targeting shRNA (Steap4-sh2) pair, 5′-CCGGGCACAGAGAGCACTATGATTCCTCGAGGAATCATAGTGCTCTCTGTGCTTTTTG-3′ and 5′-AATTCAAAAAGCACAGAGAGCACTATGATTCCTCGAGGAATCATAGTGCTCTCTGTGC-3′, was synthesized (Integrated DNA Technologies) and ligated into the AgeI/EcoRI site of the LKO.1 vector. A firefly luciferase shRNA was used as a control (5′-GCTTACGCTGAGTACTTCGA-3′). 293-T cells were cotransfected with a LKO.1 gene transfer vector and virus packaging vectors ΔH8.2 and VSVG by TransIT-LT1 transfection reagent (Mirus). Virus supernatants were collected after 48 h of transfection. BMMs were transduced with virus supernatant containing M-CSF and 20 μg/ml of protamine (Sigma-Aldrich). Cells were then selected in α-10 medium containing M-CSF and 6 μg/ml puromycin (Sigma-Aldrich) for 3 days.

Retroviral Transduction of BMMs—The HA-tagged, full-length murine Steap4 cDNA was amplified by PCR with Pfx DNA polymerase (Invitrogen) using pCMV-SPORT6-Steap4 (clone ID 3500056, Thermal Open Biosystems) as a template. The amplified cDNA was cloned into the pMX-IRES-BSR retrovirus vector. The sequence was verified by DNA sequencing. The recombinant retroviral vector was transfected into Plat E retroviral packing cells using TransIT-LT1 transfection reagent. Virus supernatant was collected at 48 h after transfection. BMMs were transduced with virus for 24 h in α-10 medium containing M-CSF and 20 μg/ml of protamine. Cells were then selected in α-10 medium containing M-CSF and 1.5 μg/ml of blasticidin (Calbiochem) for 3 days.

Tartrate-resistant Acid Phosphatase (TRAP) Staining and TRAP Activity Assay—BMMs were cultured on a 48-well tissue culture plate in α-10 medium with M-CSF and RANKL for 4–5 days. The cells were fixed with 4% paraformaldehyde/PBS, and TRAP was stained with NaK tartrate and naphthol AS-BI phosphoric acid (Sigma-Aldrich) as described previously (32).

For the measurement of TRAP activity, BMMs were cultured on a 96-well tissue culture plate in α-10 medium M-CSF and RANKL for 3–4 days. After washing twice in PBS, the cells were fixed with ethanol and acetone (1:1) for 1 min. The cells were air-dried at room temperature. 80 μl of 20 mM phosphatase substrate and 80 mM tartaric acid in 0.09 M citrate buffer were added to each well. After the cells were incubated for 15 min at room temperature, the reaction was stopped by adding 20 μl of 0.1 N NaOH to each well. The optical density at 405 nm was measured using an iMark microplate reader (Bio-Rad) (33).

Immunoblotting—Cultured cells were washed twice with ice-cold PBS and lysed in 1× radioimmune precipitation assay buffer (Sigma-Aldrich) containing 1 mM DTT and Complete Mini EDTA-free protease inhibitor mixture (Roche). After incubation on ice for 30 min, the cell lysates were clarified by centrifugation at 14,000 rpm for 15 min at 4 °C. 10–30 μg of total protein was subjected to 8% SDS-PAGE gels and transferred electrophoretically onto PVDF membrane by a semidry blotting system (Bio-Rad). The membrane was blocked in 5% fat-free milk/Tris-buffered saline for 1 h and incubated with primary antibodies at 4 °C overnight, followed by secondary antibodies conjugated with horseradish peroxidase (Santa Cruz Biotechnology). After rinsing three times with Tris-buffered saline containing 0.1% Tween 20, the membrane was subjected to Western blot analysis with enhanced chemiluminescent detection reagents (Millipore).

Immunofluorescence—Immunofluorescence was performed as described previously (34). In brief, cells grown on glass coverslips on a 24-well plate were fixed with 4% paraformaldehyde in PBS for 20 min, followed by permeabilization and blocking in PBS/0.2% BSA/0.1% saponin for 30 min. The cells were then incubated with primary antibodies in PBS/0.2% BSA/0.1% saponin for 2 h. Primary antibody labeling was visualized using fluorescent dye-conjugated secondary antibodies (Jackson ImmunoResearch Laboratories Inc.) in PBS/0.2% BSA/0.1% saponin for 45 min. F-actin was stained with Alexa Fluor 488 phalloidin (Invitrogen). The nucleus was labeled with Hoechst 33258. Samples were mounted with 80% glycerol/PBS. Immunofluorescence-labeled cells were observed using a Carl Zeiss fluorescence microscope equipped with a charge-coupled device camera.

Measurement of Cellular and Mitochondrial ROS—BMMs were cultured with M-CSF and RANKL for 3 days. 10 μM of dichlorodihydrofluorescein was added to the culture medium and then incubated for 30 min. The cells were washed twice with PBS. The released fluorescent 7-amino-4-trifluoromethylcoumarin was measured by a microplate fluorescence reader Synergy 2 (BioTek Instruments) with excitation/emission wavelengths of 485/528 nm, respectively, and recorded by Gene 5 software (35). Mitochondrial ROS was stained with 5 μM MitoSOX Red for 10 min, followed by washing three times with Hanks' buffer. Fluorescence intensity was measured by a microplate fluorescence reader Synergy 2 with excitation/emission wavelengths of 510/580 nm, respectively.

Measurement of Intracellular Labile Iron—BMMs were cultured in α-10 medium with M-CSF and RANKL for 3 days. The cells were rinsed twice with prewarmed α-MEM. The cells were loaded with PG SK (20 μM) for 10 min at 37 °C in α-MEM. After rinsing with α-MEM, 10 mM of 2,2-dipyridyl (2,2′-DPD) was added. Cellular fluorescence was recorded by Gene 5 software at the indicated time points using a microplate fluorescence reader Synergy 2 with excitation/emission wavelengths of 485/528 nm, respectively (36).

Statistics—Data of two-group comparisons were analyzed using two-tailed Student's *t* test. For all graphs and in the text, data are represented as mean ± S.D.

RESULTS

Steap4 mRNA Expression Increases during Osteoclast Differentiation—In search of molecules regulating osteoclast iron metabolism, we performed a real-time PCR experiment to examine the expression of Steap family members during oste-

oclast differentiation. As shown in Fig. 1, Steap1 and Steap2 mRNAs were undetectable in osteoclast lineage cells. Steap3, which is essential for iron metabolism in erythroid cells (14), was constantly expressed in BMMs, preosteoclasts, and mature osteoclasts. Although Steap4 mRNA was undetected in BMMs, its expression was up-regulated during osteoclast differentiation, reaching its highest level in mature cells. This result strongly suggests that Steap4 might be functionally important in osteoclast formation and/or function.

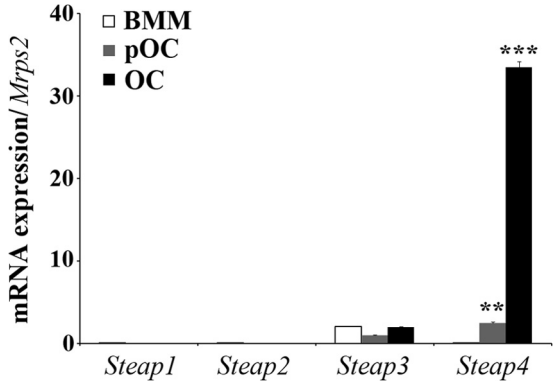

FIGURE 1. **The expression of Steap4 increases during osteoclast differentiation.** Total RNAs were purified from three independent cultures of BMMs, pOCs, and OCs, respectively. Quantitative real-time RT-PCR analysis of the expression of Steap family proteins during osteoclast differentiation was performed using TaqMan assay primers from Invitrogen. **, $p < 0.01$; ***, $p < 0.001$ *versus* BMMs by Student's *t* test.

Knockdown of Steap4 Expression in Macrophages Markedly Inhibits Osteoclast Formation—To unravel the role of Steap4 in osteoclast biology, we proceeded to knock down its expression in osteoclast lineage cells by lentiviral transduction of shRNAs (Steap4-sh1 and Steap4-sh2), specifically targeting Steap4 mRNA in BMMs. A shRNA-targeting firefly luciferase (Luc-sh) was used as a negative control. Positively transduced BMMs were then cultured with M-CSF and RANKL, and the mRNA levels of Steap4 in BMMs, preosteoclasts (pOCs), and mature osteoclasts (OCs) were measured by real-time PCR. As shown in Fig. 2*A*, Steap4 shRNAs potently inhibited Steap4 expression in pOCs and OCs without changing the expression levels of the other three Steap proteins (Fig. 2*B*). Decreased Steap4 expression resulted in markedly reduced osteoclast formation as compared with Luc-sh-transduced cells, as evidenced by the decrease of multinucleated cells staining positively for TRAP, an osteoclast differentiation marker (Fig. 2*C*). This finding was confirmed by quantitative measurement of TRAP activity (Fig. 2*D*). This measurement correlates well with the osteoclast number in osteoclast cultures (33). Moreover, the expression of osteoclast marker genes, cathepsin K (encoded by *Ctsk*), TRAP (encoded by *Acp5*), calcitonin receptor (encoded by *Calcr*), and NFATc1 (encoded by *Nfatc1*), as measured by real-time quantitative PCR, was reduced significantly in Steap4 down-regulated pOCs and OCs as compared with control cells (Fig. 3*A*). Accordingly, RANKL-induced protein expression of NFATc1 and cathepsin K was greatly reduced in Staep4-deficient osteoclast precursor cells (Fig. 3*B*). Taken together, these data indicate that Steap4 plays a critical role in osteoclastogenesis.

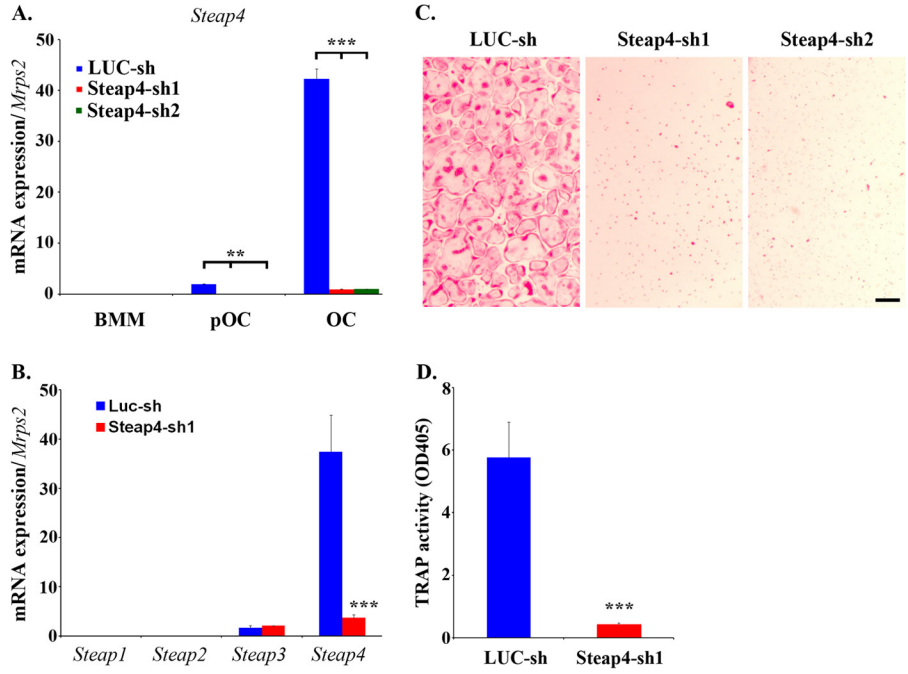

FIGURE 2. **Knockdown of Steap4 expression markedly inhibits osteoclast formation.** *A*, BMMs were transduced with recombinant lentiviruses expressing a control shRNA targeting firefly luciferase (*LUC-sh*) or two Steap4-targeting shRNAs (*Steap4-sh1* and *Steap4-sh2*), respectively. After selection with 6 μg/ml puromycin for 3 days, the cells were cultured with M-CSF alone (BMM) or M-CSF plus RANKL for 2 (pOC) and 5 days (OC). Total RNAs were isolated from three independent cultures of each group. Quantitative real-time RT-PCR analysis of the expression of Steap4 was performed. **, $p < 0.01$; ***, $p < 0.001$ *versus* LUC-sh by Student's *t* test. *B*, lentivirus-mediated transduction of a shRNA targeting Steap4 mRNA (*Steap4-sh1*) specifically and dramatically inhibits Steap4 expression without changing the expression levels of the other three Steap proteins. A shRNA targeting firefly luciferase was used as a negative control. The total RNAs were isolated from three independent cultures of each group for quantitative real-time RT-PCR analysis. *C*, lentivirus-transduced BMMs were cultured with M-CSF and RANKL for 5 days. The cells were fixed and stained for TRAP. *Scale bar* = 20 μm. *D*, decreased Steap4 expression resulted in markedly reduced osteoclast formation as compared with control cells, as demonstrated by TRAP activity assay. $n = 6$. ***, $p < 0.001$ *versus* LUC-sh by Student's *t* test.

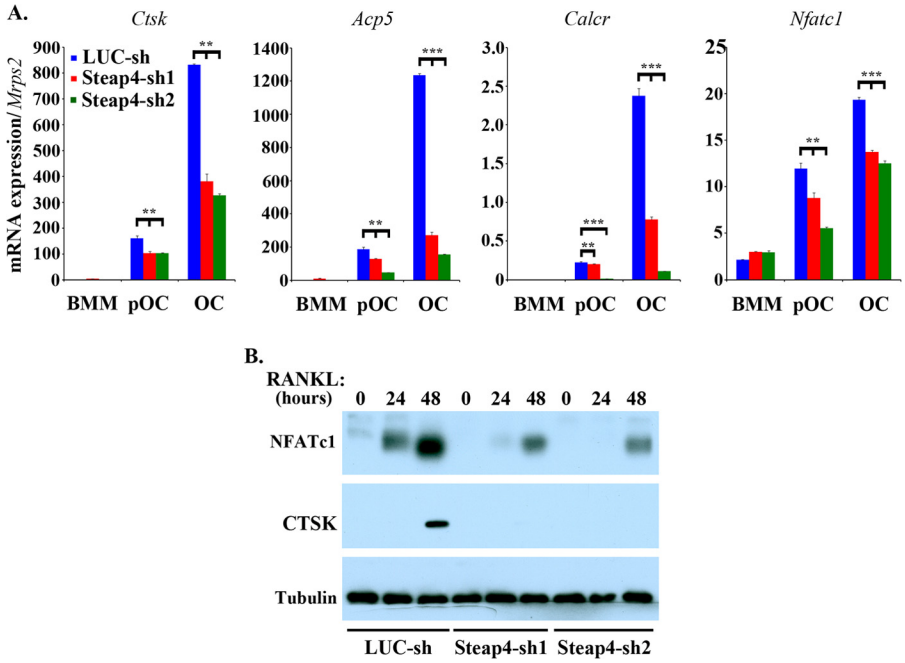

FIGURE 3. **Loss of Steap4 inhibits mRNA and protein expression of osteoclast markers.** *A*, mRNA expression of the osteoclast marker genes cathepsin K (encoded by *Ctsk*), TRAP (encoded by *Acp5*), calcitonin receptor (encoded by *Calcr*), and NFATc1 (encoded by *Nfatc1*) was measured by quantitative real-time PCR using TaqMan assay primers from Invitrogen. $n = 3$. **, $p < 0.01$; ***, $p < 0.001$ *versus* LUC-sh by Student's *t* test. *B*, lentivirus-transduced BMMs were cultured with 30 ng/ml M-CSF for 1 day, and then the cells were stimulated with 200 ng/ml RANKL for 0, 24, and 48 h. The protein expression of NFATc1 and cathepsin K was detected by Western blot analyses. Tubulin served as a loading control.

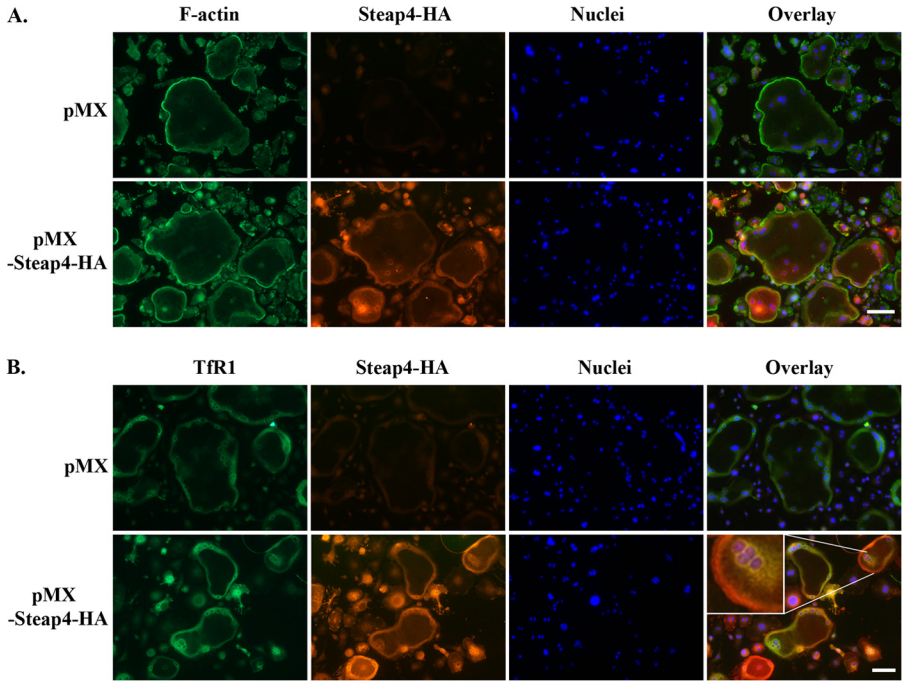

FIGURE 4. **Steap4 is predominantly localized at recycling endosomes in osteoclast lineage cells.** BMMs were transduced with a recombinant retrovirus expressing a HA-tagged murine Steap4 and were cultured with M-CSF and RANKL for 4 days before fixation. *A*, the localization of HA-tagged Steap4 was detected by monoclonal or polyclonal anti-HA antibodies. Filament actin was labeled by Alexa Fluor 488 phalloidin. A large portion of Steap4 was associated with punctate membrane structures in the cytoplasm and surrounding the nuclei in both mononuclear osteoclast precursor cells and multinucleated mature cells. *B*, Steap4 was observed to partially colocalize with TfR1 at recycling endosomes (shown in *yellow* in the *inset* of the overlay image). The empty vector (pMX)-transduced cells served as negative controls of the staining. *Scale bars* = 10 μm.

Steap4 Is Partially Colocalized with Transferrin Receptor at Recycling Endosomes in Osteoclasts—Steap4 is localized at the plasma membrane as well as endosomes in adipocytes, epithelial cells, and hematopoietic cells (13, 37). We sought to examine its distribution in osteoclasts. Because there is no high-quality anti-Steap4 antibody available for immunofluorescent staining of endogenous Steap4, we expressed the C terminus HA-tagged murine Steap4 in BMMs by retroviral transduction. Positively transduced BMMs were cultured with M-CSF and RANKL for 4 days before fixation. The localization of HA-tagged Steap4

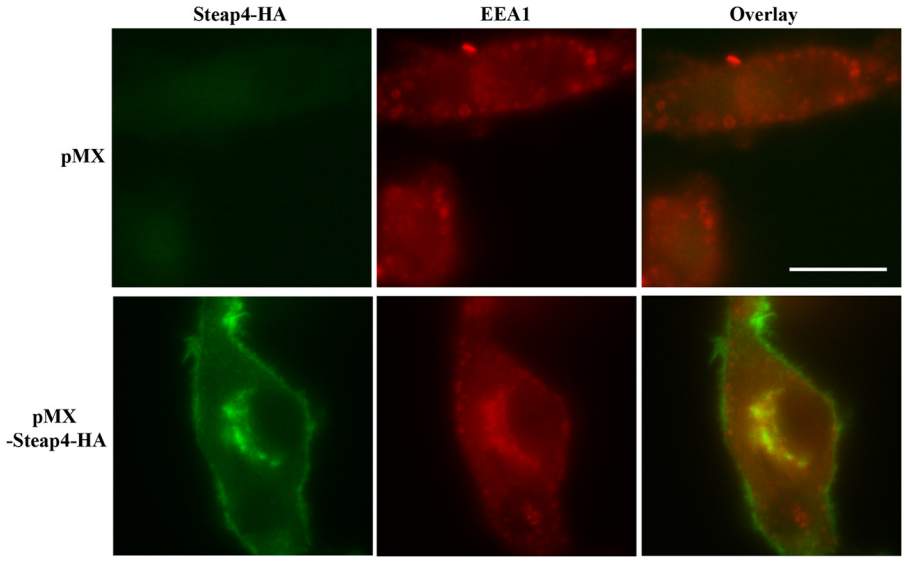

FIGURE 5. **Steap4 is not localized at early endosomes.** BMMs were transduced with a recombinant retrovirus expressing HA-tagged murine Steap4 and cultured with M-CSF and RANKL for 2 days before fixation. The localization of HA-tagged Steap4 and the early endosome marker EEA1 was detected by mouse monoclonal anti-HA (Covance) and rabbit polyclonal anti-EEA1 (Sigma-Aldrich) antibodies, respectively. Overexpressed Steap4 is not colocalized with EEA1 at early endosomes. The empty vector (pMX)-transduced cells served as negative controls of the staining. *Scale bar* = 10 μm.

was detected by monoclonal or polyclonal anti-HA antibodies. As shown in Fig. 4, *A* and *B*, a large portion of Steap4 was associated with punctate membrane structures in the cytoplasm and surrounded the nuclei in both mononuclear osteoclast precursor cells and multinucleated mature cells. To characterize the identity of these Steap4-positive organelles in osteoclast lineage cells, we performed dual immunostaining of Steap4 and TfR1, which has been shown to partially colocalize with Steap4 in other cell types and is a marker of recycling endosomes in osteoclasts (13). A high degree of colocalization (shown in *yellow* in the overlay image in Fig. 4*B*) of Steap4 and TfR1 was observed at perinuclear recycling endosomes. Overexpression of Steap4 in pOCs did not show to colocalize with the early endosomal marker, EEA1, at both peripheral and perinucleic regions (Fig. 5). These findings indicate that Steap4 resides predominantly in endosomes and may functions as a ferrireductase in osteoclast lineage cells as it does in other cells.

Down-regulation of Steap4 Expression Decreases Intracellular Iron/ROS Levels in Osteoclast Precursors—The bulk of intracellular iron is bound to proteins and enzymes, but there exists a small transition pool of chelatable iron, also called labile iron, within mammalian cells. This proportion of intracellular labile iron constitutes a balance between iron uptake and intracellular iron utilization/storage (38). Iron ions in this transition pool, in which ferrous iron is the major form, is capable of catalyzing H_2O_2 and generating highly reactive oxygen species, such as the hydroxyl radical (39). To determine whether Steap4 regulates intracellular iron metabolism in osteoclasts, we adopted a non-radioactive method of detecting intracellular chelatable iron using the fluorescent probe PG SK (36). Control and Steap4-deficient BMMs were cultured with M-CSF and RANKL for 3 days. Preosteoclasts were then loaded with PG SK, the fluorescence of which is quenched by intracellular ferrous iron, followed by an incubation with the membrane-permeable transition metal chelator 2,2′-DPD. In this system, fluorescence

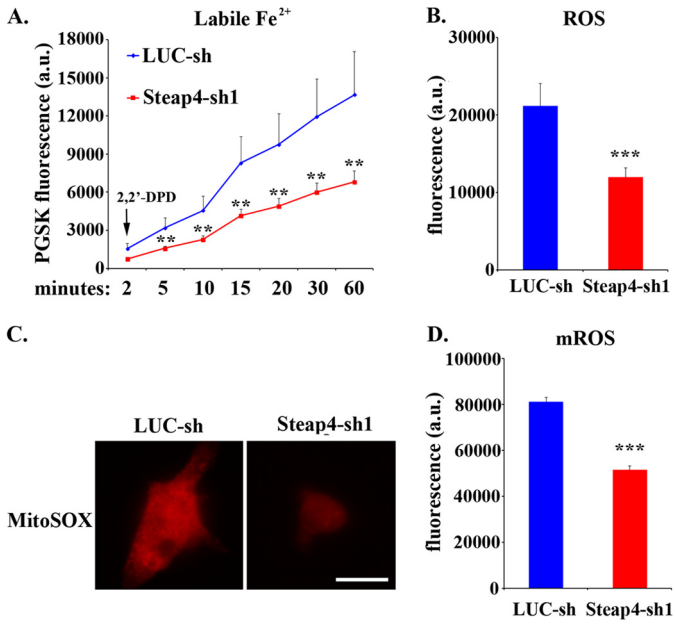

FIGURE 6. **Down-regulation of Steap4 expression decreases intracellular iron/ROS levels.** *A*, the cellular labile iron level in pOCs was reflected by the intensity of PG SK fluorescence followed by 2,2′-DPD treatment for the indicated times. $n = 6$. *B*, the cellular ROS level in lentivirus-transduced pOCs was detected using dichlorodihydrofluorescein as a probe. $n = 6$. The fluorescence intensity was measured by a microplate fluorescence reader Synergy 2 with excitation/emission wavelengths of 485/528 nm, respectively, and recorded by Gene 5 software. *C* and *D*, the level of mitochondrial ROS in lentivirus-transduced pOCs was detected using MitoSOX Red by fluorescent microscope (*C*) and a fluorescent microplate reader (*D*) with excitation/emission wavelengths of 510/580 nm, respectively. **, $p < 0.01$; ***, $p < 0.001$ *versus* LUC-sh by Student's *t* test. *Scale bar* = 20 μm. *mROS*, mitochondrion-derived ROS. *a.u.*, arbitrary units.

increases because of the removal of cellular iron from PG SK by 2,2′-DPD, and changes in fluorescence intensity, detected by a fluorescent microplate reader, correlate well with the levels of intracellular iron (36). Using this method, we found that down-regulation of Steap4 expression in osteoclast precursors led to a greater than 50% reduction in ferrous iron level (Fig. 6*A*). More-

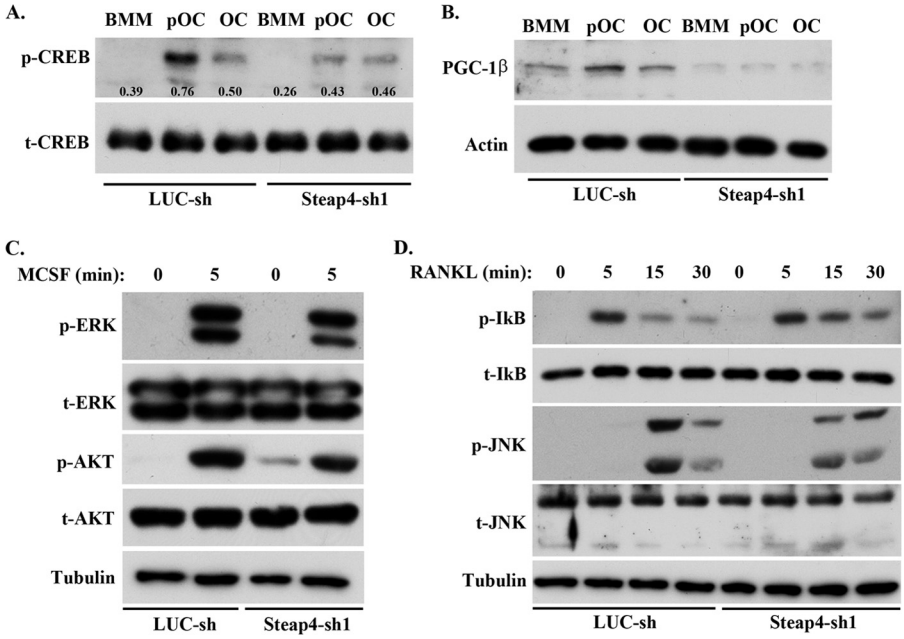

FIGURE 7. **Steap4 deficiency attenuates CREB activation and PGC-1β expression.** *A* and *B*, BMMs were cultured with M-CSF alone (BMM) or M-CSF plus RANKL for 2 (pOC) and 5 (OC) days. The cells were lysed, and the phosphorylation status of CREB (*p-CREB*) and the protein level of PGC-1β were detected by Western blot analyses. Total CREB (*t-CREB*) and actin served as loading controls, respectively. The numbers in *A* are ratios of p-CREB/t-CREB intensity measured by National Institutes of Health ImageJ software. *C* and *D*, lentivirus-transduced BMMs were serum-starved overnight and stimulated with 50 ng/ml M-CSF (*C*) and 100 ng/ml RANKL (*D*) for the indicated times. The activation of the downstream signaling pathways was detected by Western blot analyses. Tubulin served as a loading control.

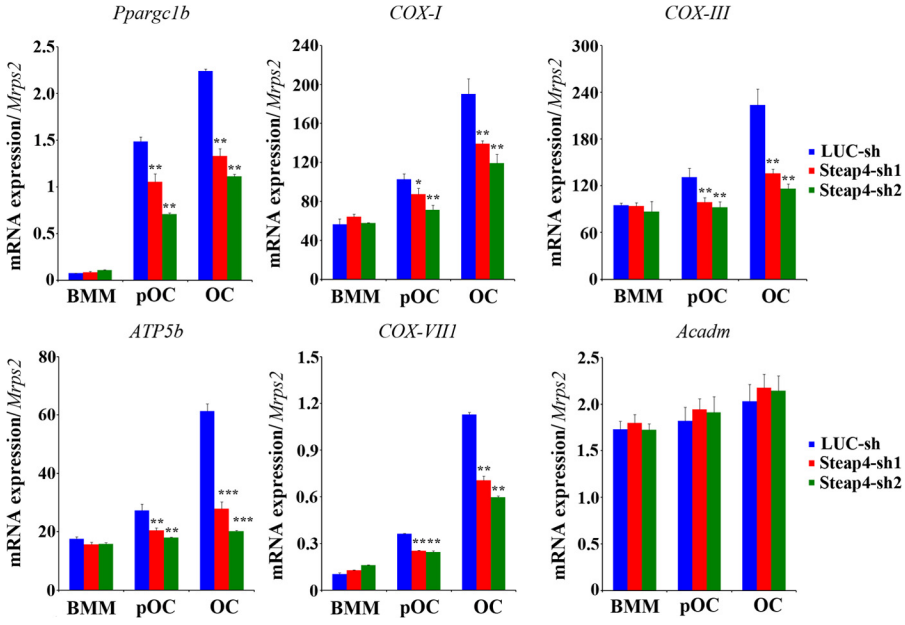

FIGURE 8. **Loss of Steap4 decreases the expression of PGC-1β and mitochondrial genes.** BMMs were transduced with lentiviruses expressing a control shRNA (*LUC-sh*) or two Steap4-targeting shRNAs (*Steap4-sh1* and *Steap4-sh2*), respectively. After puromycin selection for 3 days, the cells were cultured with M-CSF alone (BMM) or M-CSF plus RANKL for 2 (pOC) and 5 days (OC). The total RNAs were isolated from three independent cultures of each group. Quantitative real-time RT-PCR analysis of the expression of PGC-1β (encoded by Ppargc1b) and mitochondrial genes in BMMs, pOCs, and OCs was performed using TaqMan assay primers from Invitrogen. *, $p < 0.05$; **, $p < 0.01$; and ***, $p < 0.001$ *versus* LUC-sh by Student's *t* test.

over, consistent with an important role of cellular iron in ROS production in osteoclast precursor cells, knockdown of Steap4 caused a decrease in cellular and mitochondrial ROS in preosteoclasts as compared with the control cells (Fig. 6, *B–D*).

Loss of Steap4 Attenuates CREB Activation and Mitochondrion Gene Expression in Osteoclasts—Because ROS regulate the phosphorylation and activation of CREB (8), we next examined the phosphorylation status of CREB in shRNA-treated cells. CREB activation was abrogated by the absence of Steap4 in osteoclasts cultured with RANKL (Fig. 7*A*). Decreased CREB activation resulted in a significant decline in mRNA and protein expression of PGC-1β (Figs. 7*B* and 8). Accordingly, the mRNA expression of the mitochondrial genes COX-I, COX-III, ATP5b, and COX-VIIa, known downstream target genes of

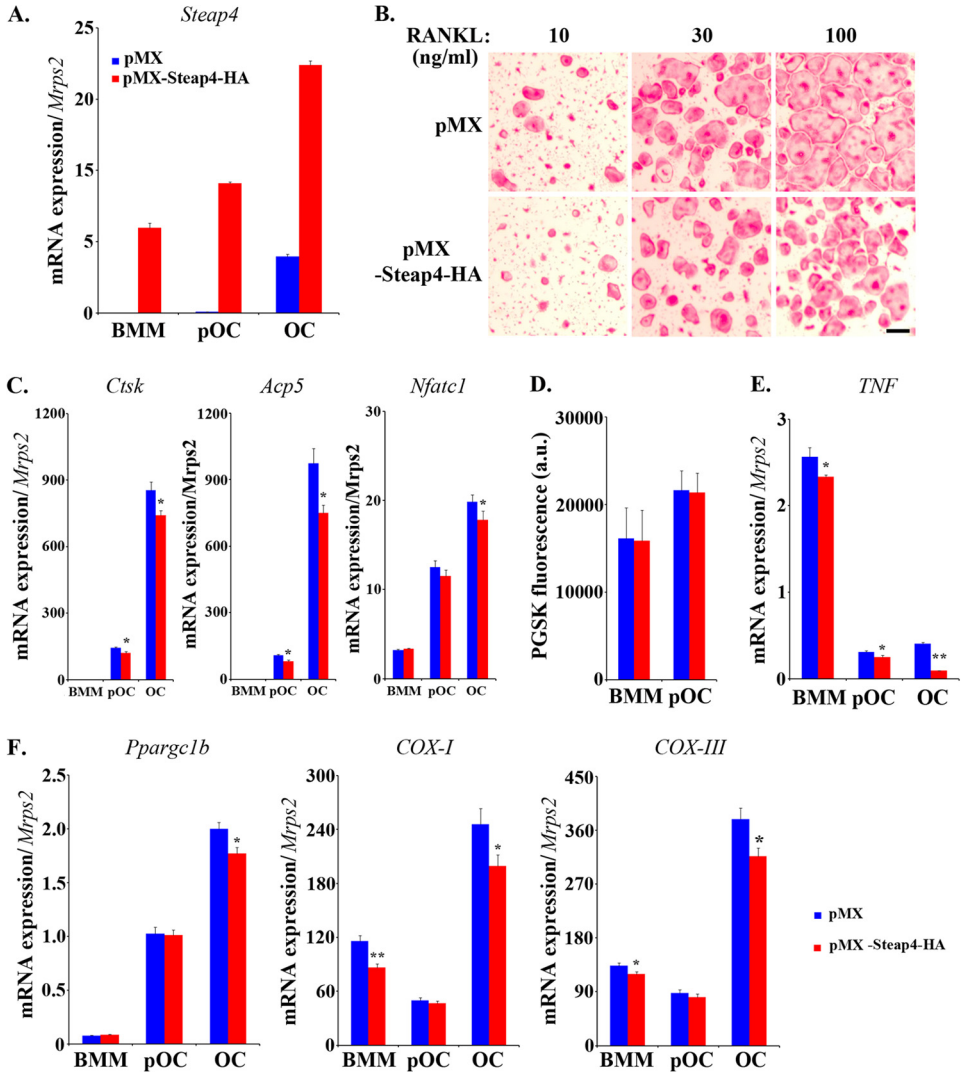

FIGURE 9. **Overexpression of Steap4 in BMMs slightly inhibits osteoclast formation.** *A*, BMMs were transduced with recombinant retroviruses expressing an empty vector (*pMX*) or HA-tagged murine Steap4 (*pMX-Steap4-HA*). After 3 days of selection with blasticidin, the cells were cultured with either M-CSF alone (BMM) or M-CSF plus RANKL for 2 days (pOC) and 5 days (OC). The total RNAs were isolated from three independent cultures of each group. Quantitative real-time RT-PCR analysis of the expression of Steap4 was performed using a TaqMan assay and a primer from Invitrogen. *B*, BMMs were cultured with M-CSF and different doses of RANKL for 5 days. The cells were fixed and stained for TRAP. *Scale bar* = 20 μm. *C*, quantitative real-time RT-PCR analysis of the expression of osteoclast marker genes was performed using RNAs isolated from three independent cultures of each group. *, $p < 0.05$ *versus* pMX by Student's *t* test. *D*, the cellular labile iron levels in BMM and pOC were measured by PG SK fluorescent dye followed by 2′2-DPD treatment for 60 min. $n = 5$. *E*, quantitative real-time RT-PCR analysis of the expression of TNF in BMMs, pOCs, and OCs. $n = 3$. *, $p < 0.05$; **. $p < 0.01$ *versus* pMX by Student's *t* test.

PGC-1β (8, 9), in preosteoclasts and mature osteoclasts was decreased (Fig. 8). In contrast, lowering cellular iron/ROS had minor effects on M-CSF-induced ERK/AKT- and RANKL-stimulated NF-κB/JNK activation (Fig. 7, *C* and *D*).

Nonetheless, overexpression of Steap4 in osteoclast precursors did not increase cellular iron nor did it accelerate osteoclast differentiation. Instead, overexpression of Steap4 in BMMs, which normally do not express Steap4, slightly inhibited osteoclast formation, as evidenced by decreased TRAP staining and the mRNA abundance of several osteoclast marker genes (Fig. 9, *A*–*C*). The most likely explanation for this seemingly incongruent finding is that in BMMs and pOCs, Steap4 and/or Steap3 are sufficient to meet the iron uptake demands. Interestingly, Steap4 overexpression also induced an iron-independent reduction in mRNA expression of TNF, a pivotal inflammatory cytokine that synergistically enhances RANKL-induced osteoclast differentiation *in vitro* and *in vivo* (40). Therefore, it is likely that the decreased TNF expression in Steap4-overexpressing osteoclast lineage cells contributed to the attenuation of osteoclast differentiation. Future work will be required to determine whether Steap4 plays a role in bone homeostasis *in vivo*. Notably, global deletion of Steap4 in mice causes overt inflammation and glucose deregulation, but the skeletal phenotype of this mouse model has not been examined (19).

DISCUSSION

Iron uptake via the Tf cycle, in concert with PGC-1β, regulates mitochondrial biogenesis, ROS production, and CREB activation during osteoclastogenesis (8). However, the molecular mechanisms controlling cellular iron metabolism in osteoclasts remain largely unknown. A rate-limiting step in intra-

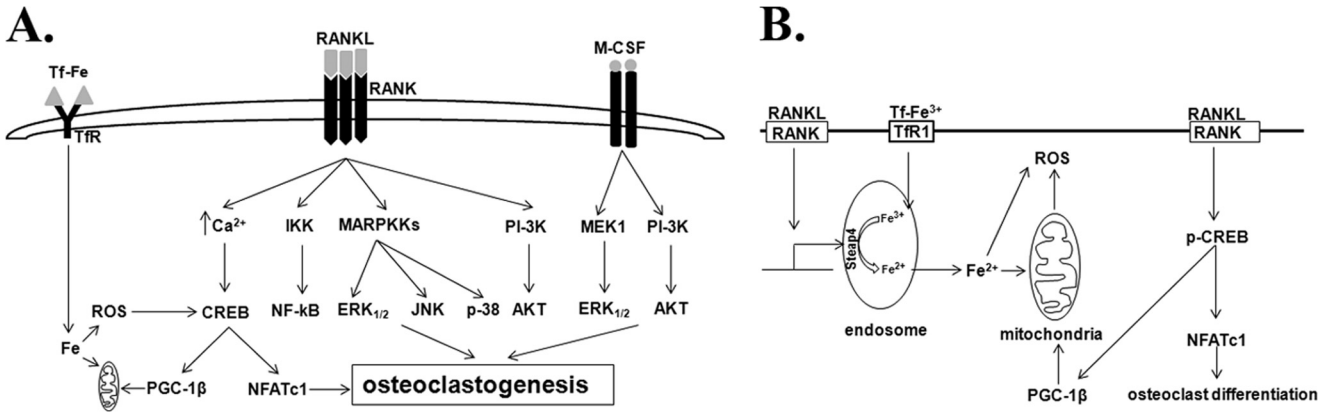

FIGURE 10. **Schematics of signaling pathways and a model of Steap4 function in osteoclast differentiation.**

cellular iron trafficking and utilization is the reduction of ferric iron to ferrous iron, which is carried out by Steap family proteins (11). Three of four family members, Steap2, Steap3, and Steap4, are ferrireductases and cupric reductases that stimulate cellular uptake of both iron and copper in mammalian cells (13). Relative to Steap2 and Steap3, Steap4 is highly expressed in bone marrow and has the highest metalloreductase activities (13). The results of this work have elucidated that expression of Steap4 is up-regulated during osteoclast differentiation. By contrast, knockdown of Steap4 expression in osteoclast precursor cells markedly inhibited osteoclast differentiation. This was associated with lower intracellular iron and ROS levels and led to the attenuation of CREB activation. Moreover, in line with previous reports (8, 9), induction of PGC1-β/mitochondrial mRNA expression, two downstream pathways regulated by CREB, were also attenuated by knockdown of Steap4. Our work also revealed that Steap2 is not expressed in osteoclast lineage cells and that the expression of Steap3 is constant but at lower levels than that of Steap4. Therefore, Steap4 must be the critical endosomal ferrireductase for osteoclast differentiation. On the basis of these findings, we have concluded that Steap4, in conjunction with the Tf/TfR pathway, promotes cellular iron uptake and utilization required for osteoclast development and function (Fig. 10). These data strongly suggest that Steap4 plays an essential role in regulating cellular iron metabolism, ROS production, and CREB/PGC-1 β activation in osteoclast precursors and mature cells.

Lee and co-workers (26) have reported that RANKL stimulation of osteoclast precursor cells activates the Rac1/NADPH oxidase (Nox) pathway and, therefore, enhances ROS production. This, in turn, plays a crucial role in RANKL-induced activation of MAPKs (ERK, JNK, and p38), NF-κB, and the PI3K/AKT pathways (26). We show here that down-regulation of Steap4 expression in osteoclast lineage cells dramatically decreased iron/ROS levels and markedly inhibited osteoclast differentiation. However, the decrease in ROS caused by iron deficiency in osteoclast precursors in this work had minor effects on canonical RANKL signaling. Instead, it dramatically decreased CREB activation and PGC-1β expression. The difference in the effects of ROS on RANKL signaling in our study *versus* the studies by Lee *et al.* (24, 26) most likely reflects distinct subcellular sites of ROS generation (*e.g.* mitochondria *versus* plasma membrane, respectively). In support of this notion, Steap4 deficiency causes a decline in mitochondria-derived ROS to a similar degree as total cellular ROS (Fig. 6, *B* and *D*). Specifically, generation of ROS by the Rac1/Nox pathway occurs near the plasma membrane and, thus, it might modulate proximal events of the RANKL/RANK signaling pathways. On the other hand, the cellular iron level is critical for mitochondrial biogenesis and function. Hence, a decrease in ROS as a result of iron deficiency may result from the decrease of mitochondrion-derived ROS, which affect the distal components of RANKL/RANK signaling, *i.e.* the calmodulin-dependent kinase/CREB pathway. Consistent with this scenario, loss of calmodulin-dependent kinase IV and Tmem65 in osteoclast precursors inhibits CREB activation and osteoclast differentiation without changing RANKL-induced ERK, JNK, and NF-κB activation (6, 41). Future studies will be required to delineate the differential roles of Nox-induced ROS and mitochondria-derived ROS in osteoclast differentiation and function.

It has been long recognized that iron overload causes loss of bone mass and fractures in patients with hemochromatosis, hemosiderosis, thalassemia, and sickle cell disease (42). Iron accumulation and toxicity are also major side effects of chronic red blood cell transfusion in patients with congenital or acquired anemia (43). The adverse effects of iron overload on bone have been attributed to an imbalance in bone remodeling caused by an increase in osteoclastic bone resorption and a decrease in osteoblastic bone formation because of an increase in oxidative stress (28, 44, 45). In support of a role of ROS as critical culprits in these pathologic conditions, the results of this work, along with the work of Ishii *et al.* (8), indicate that Steap4 and the Tf/TfR pathway are indeed essential for iron uptake and utilization during osteoclastogenesis because of their ability to stimulate mitochondrial biogenesis/function and ROS production. ROS, in turn, activate the calmodulin-dependent kinase/CREB pathway and enhance osteoclast differentiation and function in response to RANKL. In another work of ours, we have elucidated that, in contrast to the requirement of ROS for osteoclastogenesis, oxidative stress suppresses osteoblast differentiation and bone formation by inducing FoxO transcription factors, which bind to and divert β-catenin from canonical Wnt signaling (46, 47). Taking these lines of evidence together, we submit that decreased ROS production in general, and targeting Steap4 and/or components of the

Tf/TfR pathway in particular, may represent rational therapeutic strategies for bone diseases caused by iron overload.

Acknowledgments—We thank Drs. Robert L. Jilka and Charles A. O'Brian for critical reading of the manuscript prior to submission. We also thank Dr. Yunfeng Feng for help with Steap4 shRNA design and Erin Hogan for support with microscopes.

REFERENCES

1. Boyle, W. J., Simonet, W. S., and Lacey, D. L. (2003) Osteoclast differentiation and activation. *Nature* **423,** 337–342
2. Teitelbaum, S. L. (2000) Bone resorption by osteoclasts. *Science* **289,** 1504–1508
3. Helfrich, M. H. (2003) Osteoclast diseases. *Microscopy Res. Tech.* **61,** 514–532
4. Suda, T., Takahashi, N., Udagawa, N., Jimi, E., Gillespie, M. T., and Martin, T. J. (1999) Modulation of osteoclast differentiation and function by the new members of the tumor necrosis factor receptor and ligand families. *Endocr. Rev.* **20,** 345–357
5. Ross, F. P., and Teitelbaum, S. L. (2005) $\alpha v\beta 3$ and macrophage colony-stimulating factor. Partners in osteoclast biology. *Immunol. Rev.* **208,** 88–105
6. Sato, K., Suematsu, A., Nakashima, T., Takemoto-Kimura, S., Aoki, K., Morishita, Y., Asahara, H., Ohya, K., Yamaguchi, A., Takai, T., Kodama, T., Chatila, T. A., Bito, H., and Takayanagi, H. (2006) Regulation of osteoclast differentiation and function by the CaMK-CREB pathway. *Nat. Med.* **12,** 1410–1416
7. Takayanagi, H., Kim, S., Koga, T., Nishina, H., Isshiki, M., Yoshida, H., Saiura, A., Isobe, M., Yokochi, T., Inoue, J., Wagner, E. F., Mak, T. W., Kodama, T., and Taniguchi, T. (2002) Induction and activation of the transcription factor NFATc1 (NFAT2) integrate RANKL signaling in terminal differentiation of osteoclasts. *Dev. Cell* **3,** 889–901
8. Ishii, K. A., Fumoto, T., Iwai, K., Takeshita, S., Ito, M., Shimohata, N., Aburatani, H., Taketani, S., Lelliott, C. J., Vidal-Puig, A., and Ikeda, K. (2009) Coordination of PGC-1β and iron uptake in mitochondrial biogenesis and osteoclast activation. *Nat. Med.* **15,** 259–266
9. Wei, W., Wang, X., Yang, M., Smith, L. C., Dechow, P. C., Sonoda, J., Evans, R. M., and Wan, Y. (2010) PGC1β mediates PPARγ activation of osteoclastogenesis and rosiglitazone-induced bone loss. *Cell Metab.* **11,** 503–516
10. Chen, C., and Paw, B. H. (2012) Cellular and mitochondrial iron homeostasis in vertebrates. *Biochim. Biophys. Acta* **1823,** 1459–1467
11. Pantopoulos, K., Porwal, S. K., Tartakoff, A., and Devireddy, L. (2012) Mechanisms of mammalian iron homeostasis. *Biochemistry* **51,** 5705–5724
12. Knutson, M. D. (2007) Steap proteins. Implications for iron and copper metabolism. *Nutr. Rev.* **65,** 335–340
13. Ohgami, R. S., Campagna, D. R., McDonald, A., and Fleming, M. D. (2006) The Steap proteins are metalloreductases. *Blood* **108,** 1388–1394
14. Ohgami, R. S., Campagna, D. R., Greer, E. L., Antiochos, B., McDonald, A., Chen, J., Sharp, J. J., Fujiwara, Y., Barker, J. E., and Fleming, M. D. (2005) Identification of a ferrireductase required for efficient transferrin-dependent iron uptake in erythroid cells. *Nat. Genet.* **37,** 1264–1269
15. Hubert, R. S., Vivanco, I., Chen, E., Rastegar, S., Leong, K., Mitchell, S. C., Madraswala, R., Zhou, Y., Kuo, J., Raitano, A. B., Jakobovits, A., Saffran, D. C., and Afar, D. E. (1999) STEAP. A prostate-specific cell-surface antigen highly expressed in human prostate tumors. *Proc. Natl. Acad. Sci. U.S.A.* **96,** 14523–14528
16. Wang, L., Jin, Y., Arnoldussen, Y. J., Jonson, I., Qu, S., Maelandsmo, G. M., Kristian, A., Risberg, B., Waehre, H., Danielsen, H. E., and Saatcioglu, F. (2010) STAMP1 is both a proliferative and an antiapoptotic factor in prostate cancer. *Cancer Res.* **70,** 5818–5828
17. Arner, P., Stenson, B. M., Dungner, E., Näslund, E., Hoffstedt, J., Ryden, M., and Dahlman, I. (2008) Expression of six transmembrane protein of prostate 2 in human adipose tissue associates with adiposity and insulin resistance. *J. Clin. Endocrinol. Metab.* **93,** 2249–2254
18. Zhang, C. M., Chi, X., Wang, B., Zhang, M., Ni, Y. H., Chen, R. H., Li, X. N., and Guo, X. R. (2008) Downregulation of STEAP4, a highly-expressed TNF-α-inducible gene in adipose tissue, is associated with obesity in humans. *Acta Pharmacol. Sin.* **29,** 587–592
19. Wellen, K. E., Fucho, R., Gregor, M. F., Furuhashi, M., Morgan, C., Lindstad, T., Vaillancourt, E., Gorgun, C. Z., Saatcioglu, F., and Hotamisligil, G. S. (2007) Coordinated regulation of nutrient and inflammatory responses by STAMP2 is essential for metabolic homeostasis. *Cell* **129,** 537–548
20. Richardson, D. R., Lane, D. J., Becker, E. M., Huang, M. L., Whitnall, M., Suryo Rahmanto, Y., Sheftel, A. D., and Ponka, P. (2010) Mitochondrial iron trafficking and the integration of iron metabolism between the mitochondrion and cytosol. *Proc. Natl. Acad. Sci. U.S.A.* **107,** 10775–10782
21. Finkel, T., and Holbrook, N. J. (2000) Oxidants, oxidative stress and the biology of ageing. *Nature* **408,** 239–247
22. Finkel, T. (2011) Signal transduction by reactive oxygen species. *J. Cell Biol.* **194,** 7–15
23. Murphy, M. P., Holmgren, A., Larsson, N. G., Halliwell, B., Chang, C. J., Kalyanaraman, B., Rhee, S. G., Thornalley, P. J., Partridge, L., Gems, D., Nyström, T., Belousov, V., Schumacker, P. T., and Winterbourn, C. C. (2011) Unraveling the biological roles of reactive oxygen species. *Cell Metab.* **13,** 361–366
24. Ha, H., Kwak, H. B., Lee, S. W., Jin, H. M., Kim, H. M., Kim, H. H., and Lee, Z. H. (2004) Reactive oxygen species mediate RANK signaling in osteoclasts. *Exp. Cell Res.* **301,** 119–127
25. Kim, M. S., Yang, Y. M., Son, A., Tian, Y. S., Lee, S. I., Kang, S. W., Muallem, S., and Shin, D. M. (2010) RANKL-mediated reactive oxygen species pathway that induces long lasting Ca^{2+} oscillations essential for osteoclastogenesis. *J. Biol. Chem.* **285,** 6913–6921
26. Lee, N. K., Choi, Y. G., Baik, J. Y., Han, S. Y., Jeong, D. W., Bae, Y. S., Kim, N., and Lee, S. Y. (2005) A crucial role for reactive oxygen species in RANKL-induced osteoclast differentiation. *Blood* **106,** 852–859
27. Lean, J. M., Davies, J. T., Fuller, K., Jagger, C. J., Kirstein, B., Partington, G. A., Urry, Z. L., and Chambers, T. J. (2003) A crucial role for thiol antioxidants in estrogen-deficiency bone loss. *J. Clin. Invest.* **112,** 915–923
28. Manolagas, S. C. (2010) From estrogen-centric to aging and oxidative stress. A revised perspective of the pathogenesis of osteoporosis. *Endocr. Rev.* **31,** 266–300
29. Ye, S., Fowler, T. W., Pavlos, N. J., Ng, P. Y., Liang, K., Feng, Y., Zheng, M., Kurten, R., Manolagas, S. C., and Zhao, H. (2011) LIS1 regulates osteoclast formation and function through its interactions with dynein/dynactin and Plekhm1. *PloS ONE* **6,** e27285
30. Takeshita, S., Kaji, K., and Kudo, A. (2000) Identification and characterization of the new osteoclast progenitor with macrophage phenotypes being able to differentiate into mature osteoclasts. *J. Bone Miner. Res.* **15,** 1477–1488
31. Schmittgen, T. D., and Livak, K. J. (2008) Analyzing real-time PCR data by the comparative C(T) method. *Nat. Protoc.* **3,** 1101–1108
32. Jilka, R. L., Hangoc, G., Girasole, G., Passeri, G., Williams, D. C., Abrams, J. S., Boyce, B., Broxmeyer, H., and Manolagas, S. C. (1992) Increased osteoclast development after estrogen loss. Mediation by interleukin-6. *Science* **257,** 88–91
33. Kirstein, B., Chambers, T. J., and Fuller, K. (2006) Secretion of tartrate-resistant acid phosphatase by osteoclasts correlates with resorptive behavior. *J. Cell. Biochem.* **98,** 1085–1094
34. Zhao, H., Laitala-Leinonen, T., Parikka, V., and Väänänen, H. K. (2001) Downregulation of small GTPase Rab7 impairs osteoclast polarization and bone resorption. *J. Biol. Chem.* **276,** 39295–39302
35. Almeida, M., Han, L., Martin-Millan, M., Plotkin, L. I., Stewart, S. A., Roberson, P. K., Kousteni, S., O'Brien, C. A., Bellido, T., Parfitt, A. M., Weinstein, R. S., Jilka, R. L., and Manolagas, S. C. (2007) Skeletal involution by age-associated oxidative stress and its acceleration by loss of sex steroids. *J. Biol. Chem.* **282,** 27285–27297
36. Petrat, F., Rauen, U., and de Groot, H. (1999) Determination of the chelatable iron pool of isolated rat hepatocytes by digital fluorescence microscopy using the fluorescent probe, Phen green SK. *Hepatology* **29,** 1171–1179
37. Korkmaz, C. G., Korkmaz, K. S., Kurys, P., Elbi, C., Wang, L., Klokk, T. I.,

Hammarstrom, C., Troen, G., Svindland, A., Hager, G. L., and Saatcioglu, F. (2005) Molecular cloning and characterization of STAMP2, an androgen-regulated six transmembrane protein that is overexpressed in prostate cancer. *Oncogene* **24,** 4934–4945
38. Ryan, T. P., and Aust, S. D. (1992) The role of iron in oxygen-mediated toxicities. *Crit. Rev. Toxicol.* **22,** 119–141
39. Stohs, S. J., and Bagchi, D. (1995) Oxidative mechanisms in the toxicity of metal ions. *Free Radic. Biol. Med.* **18,** 321–336
40. Lam, J., Takeshita, S., Barker, J. E., Kanagawa, O., Ross, F. P., and Teitelbaum, S. L. (2000) TNF-α induces osteoclastogenesis by direct stimulation of macrophages exposed to permissive levels of RANK ligand. *J. Clin. Invest.* **106,** 1481–1488
41. Kim, H., Kim, T., Jeong, B. C., Cho, I. T., Han, D., Takegahara, N., Negishi-Koga, T., Takayanagi, H., Lee, J. H., Sul, J. Y., Prasad, V., Lee, S. H., and Choi, Y. (2013) Tmem64 modulates calcium signaling during RANKL-mediated osteoclast differentiation. *Cell Metab.* **17,** 249–260
42. Li, G. F., Pan, Y. Z., Sirois, P., Li, K., and Xu, Y. J. (2012) Iron homeostasis in osteoporosis and its clinical implications. *Osteoporos. Int.* **23,** 2403–2408
43. Fleming, R. E., and Ponka, P. (2012) Iron overload in human disease. *N. Engl. J. Med.* **366,** 348–359
44. Haidar, R., Musallam, K. M., and Taher, A. T. (2011) Bone disease and skeletal complications in patients with β thalassemia major. *Bone* **48,** 425–432
45. Tsay, J., Yang, Z., Ross, F. P., Cunningham-Rundles, S., Lin, H., Coleman, R., Mayer-Kuckuk, P., Doty, S. B., Grady, R. W., Giardina, P. J., Boskey, A. L., and Vogiatzi, M. G. (2010) Bone loss caused by iron overload in a murine model. Importance of oxidative stress. *Blood* **116,** 2582–2589
46. Almeida, M., Han, L., Martin-Millan, M., O'Brien, C. A., and Manolagas, S. C. (2007) Oxidative stress antagonizes Wnt signaling in osteoblast precursors by diverting β-catenin from T cell factor- to forkhead box *O*-mediated transcription. *J. Biol. Chem.* **282,** 27298–27305
47. Manolagas, S. C., and Almeida, M. (2007) Gone with the Wnts. β-Catenin, T-cell factor, forkhead box O, and oxidative stress in age-dependent diseases of bone, lipid, and glucose metabolism. *Mol. Endocrinol.* **21,** 2605–2614